

*Supplementary material for the following manuscript submitted to the
journal*

RSC Polymer Chemistry

Design and Synthesis of Amphiphilic Statistical Copolymers Forming Unimeric
Micelles with Thermoresponsive Behaviour in the Physiological Range

Florian Tondock¹, David Nash¹, Cathleen Hudziak², Kai Ludwig², Marie Weinhart^{1,2,*}

¹ Institute of Physical Chemistry and Electrochemistry, Leibniz Universität Hannover, Callinstr.
3A, 30167 Hannover

² Institute of Chemistry and Biochemistry, Freie Universität Berlin, Takustr. 3, 14195 Berlin

* Corresponding author: marie.weinhart@pci.uni-hannover.de and marie.weinhart@fu-berlin.de

Table of Contents

1. Materials and Methods	1
2. Cu(0)-mediated synthesis of P(OEGA-co-BA) and characterisation	4
2.1 Summary of optimised reaction conditions	4
2.2 Copolymer characterisation by ¹ H NMR	5
2.3 Determination of monomer conversion from ¹ H NMR spectra	7
2.4 Change in refractive index with copolymer concentration	9
2.5 Optimisation of copolymerisation parameters	10
3. Kinetics of the copolymerisation of OEGA and BA	11
3.1 Controlled copolymerisation	11
3.2 Determination of the reactivity ratios by the Fineman-Ross approach ^[2-4]	12
3.3 Determination of the reactivity ratios by the extended Kelen-Tüdös approach ^[3,5,6]	13
4. GPC traces in tetrahydrofuran and water	15
5. Optimisation of the copolymer purification process	16
6. Cell compatibility testing of P(OEGA-co-BA)	18
7. Micelle formation in water evidenced by ¹ H NMR spectroscopy	20
8. Determination of the copolymers' association number in water ^[8,9]	21
9. Dynamic light scattering (DLS) measurements during dilution	22
10. Rheology of copolymers P(OEGA-co-BA) to determine their intrinsic viscosity	24
11. Turbidity measurements of copolymers	25
12. DLS measurements of copolymers below and above their T_{cp}	25
13. Determination of maximum micelle loading capacity	27

14. Turbidity and fluorescence measurements of pyrene-loaded micelles.....	30
15. DLS measurements of pyrene-loaded micelles.....	31
References.....	33

1. Materials and Methods

Materials. *n*-Butyl acrylate (BA, 99%) and oligo (ethylene glycol) methyl ether acrylate (OEGA, $M_n = 480 \text{ g mol}^{-1}$) were purchased from TCI GmbH (Eschborn, Germany); acetic acid (AcOH, 99%), aluminum oxide (basic), aluminum oxide (neutral), copper(II) bromide (CuBr_2 , 99%), dichloromethane (DCM, extra pure), *N,N*-dimethylformamide (DMF, analytic grade), ethylene glycol (99%), hydrochloric acid (37%), methanol (MeOH, analytic grade), molecular sieve (3 Å), phosphate-buffered saline (PBS, pH = 7.45), pentane (analytic grade), pyrene (98%), sodium bicarbonate (99%), sodium chloride (99.5%), tetrahydrofuran (THF, HPLC grade), tris[2-(dimethylamino)ethyl]amine (Me_6TREN , 99%), disposable polystyrene cuvettes and polytetrafluoroethylene (PTFE) syringe filters (0.2 μm) were from Fisher Scientific GmbH (Schwerte, Germany) and 2-bromo-isobutyryl bromide (98%), chloroform-*d* (99.8 atom%D), ethylenediamine tetraacetic acid disodium salt dihydrate (EDTA, 99%) and magnesium sulfate (extra dry, 98%) from Merck KGaA/Sigma Aldrich (Darmstadt/Steinheim, Germany). Triethylamine (99%) was supplied by abcr GmbH (Karlsruhe, Germany) and ethanol (99%) by Th. Geyer GmbH & Co. KG (Renningen, Germany). Ammonium chloride (NH_4Cl , 99%), deuterium oxide (99.9 atom%D), dialysis membrane Spectra/Por® 6 (MWCO = 1 and 3.5 KDa), and cellulose acetate (CA) syringe filters (0.45 μm) were received from Carl Roth GmbH + Co. KG (Karlsruhe, Germany).

Caco-2 cells were purchased from ATCC (HTB-37). 3-(4,5-Dimethylthiazol-2-yl)-2,5-diphenyl tetrazolium bromide (MTT) was purchased from Invitrogen (Waltham, MA, USA), 96-well TCPS plates and isopropanol (*i*-PrOH, analytic grade) from Fisher Scientific GmbH (Schwerte, Germany), fetal bovine serum (FBS) Standard from PAN-Biotech GmbH (Aidenbach, Germany), minimum essential media (MEM) from Serana Europe GmbH (Brandenburg, Germany), penicillin/streptomycin solution from Merck KGaA/Sigma Aldrich (Darmstadt/Steinheim, Germany), pyruvate solution from Carl Roth GmbH + Co. KG (Karlsruhe, Germany), and trypsin-EDTA from Biowest (Nuaille, France).

A copper standard (1 g L^{-1}) was supplied by Merck KGaA/Sigma Aldrich (Darmstadt/Steinheim, Germany).

Ethanol was distilled under reduced pressure prior to use. Copper(0) wire ($d = 0.15 \text{ mm}$, $l = 30 \text{ cm}$) was pre-treated by washing in hydrochloric acid (37%) for 20 min, then rinsed with acetone, dried under vacuum and used immediately. 1,2-Bis(2'-bromoisobutyryloxy)ethane (2f-BiB) was synthesised as reported in the literature.^[1] All other reagents and solvents were obtained at the highest purity available from Fisher Scientific GmbH, Merck KGaA/Sigma Aldrich, or TCI GmbH and used without further purification unless specified otherwise.

Atomic absorption spectroscopy (AAS). AAS was performed on a VARIAN AA140 (Varian Medical Systems, Inc., Palo Alto, United States) in an acetylene (3.5 L min^{-1})/air (1.5 L min^{-1}) flame at 324.8 nm with a measurement time of 5 s per sample to determine the remaining copper catalyst concentration in the copolymers ($n = 7$). Samples were prepared by dissolving the copolymers in ultra-pure water ($c = 10 \text{ mg mL}^{-1}$). Five standard solutions with defined Cu(0) concentrations were used to obtain a standard curve for the subsequent quantification of the copper concentration.

MTT Assay. Caco-2 cells were cultured in MEM with 20% FBS, 1% pyruvate, and 1% penicillin/streptomycin at 37 °C and 5% CO₂ in a humidified atmosphere. Cells were routinely passaged at a confluency of 80% using trypsin-EDTA and used for experiments in passages 42 to 47. For the MTT assay, the polymers were dissolved in cell culture medium. Cells were seeded onto 96-well plates at a density of 5 000 cells per well and allowed to adhere overnight. Afterwards, the culture medium was replaced by the polymer solution (0.001, 0.01, 0.1, 1 and 10 mg mL^{-1}) and incubated for up to 48 h at 37 °C. For viability measurements, the polymer solution was exchanged by pure medium and MTT reagent in medium (10 μL , 5 mg mL^{-1}) was added per well and incubated at 37 °C under cell culture conditions for 4 h. To stop the assay, 0.04 M HCl in isopropanol (100 μL) was added to each well. Subsequently,

absorption was measured at 570 nm using a Cytation 5 (Agilent Technologies, Santa Clara, USA). Untreated and DMSO-treated cells served as negative and positive controls.

Fluorescence spectroscopy. Fluorescence measurements were performed in a FluoroMax Plus spectrometer from HORIBA Scientific (Palaiseau, France) in glass cuvettes at room temperature. Fluorescence emission spectra of **P5-P7, P12** (10 mg mL^{-1}) were recorded using an excitation wavelength of $\lambda_{\text{ex}} = 337 \pm 1 \text{ nm}$, and the maximum intensities of the first and third vibronic band $I_1 = 373 \text{ nm}$ and $I_3 = 384 \text{ nm}$ were put in proportion to obtain the so-called pyrene 1:3 ratio.

2. Cu(0)-mediated synthesis of P(OEGA-co-BA) and characterisation

2.1 Summary of optimised reaction conditions

Table S1. Reaction conditions for the synthesis of P1-P12.

polymer	M_n^a [kDa]	OEGA [mmol]	BA [mmol]	2f-BiB [μ mol]	CuBr ₂ [μ mol]	Me ₆ TREN [μ mol]	[OEGA+BA]/DMF [v/v]
P1	10	16.4	16.4	1037.2	29.0	104.8	1/1
P2	50	16.4	16.4	201.5	5.6	20.3	1/1
P3	100	16.4	16.4	100.4	3.9	14.1	1/1
P4	500	16.4	16.4	20.0	1.0	3.6	1/1
P5	1 000	16.4	16.4	10.0	0.5	1.8	1/1
P6	1 000	14.9	22.3	10.0	0.5	1.8	1/1
P7	1 000	12.8	30.0	10.0	0.5	1.8	1/1
P8	1 000	12.4	31.8	10.0	0.5	1.8	1/1
P9	1 000	11.8	33.7	10.0	0.5	1.8	1/1
P10	1 000	11.3	35.7	10.0	0.5	1.8	1/1
P11	1 000	10.7	37.9	10.0	0.5	1.8	1/1
P12	1 000	10.1	40.3	10.0	0.5	1.8	1/1

^atargeted molecular weight.

2.2 Copolymer characterisation by ^1H NMR

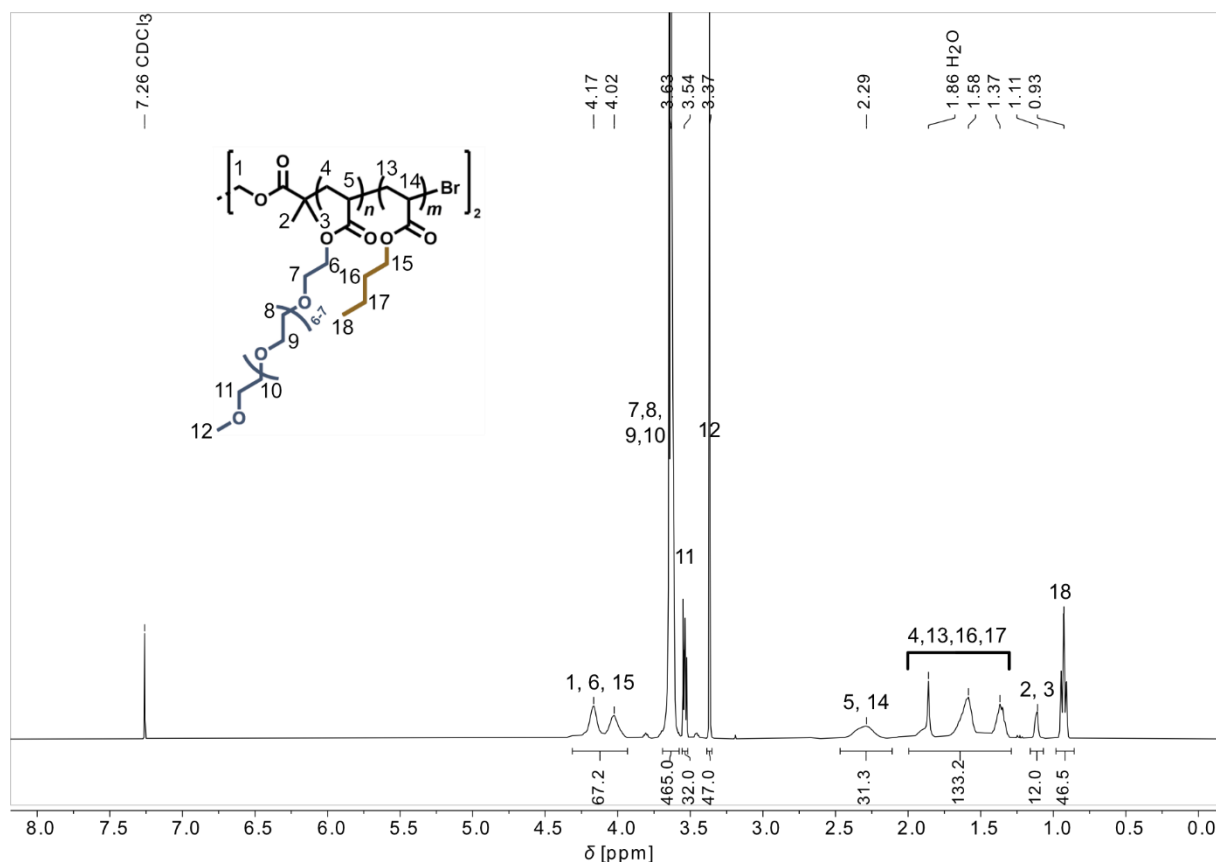


Figure S1. Representative ^1H NMR spectrum of copolymer **P1** in CDCl_3 with assigned peaks after purification according to protocol D2 (see **Table S5**).

The assignment of the individual proton signals based on Fig. S1 is outlined below for **P1-P12**.

^1H NMR (400 MHz, CDCl_3 , δ):

P1: 4.26-3.92 (m, 71H, 1- CH_2 + 6- CH_2 + 15- CH_2); 3.69-3.58 (m, 486H, 7- CH_2 + 8- CH_2 + 9- CH_2 + 10- CH_2); 3.56-3.51 (m, 34H, 11- CH_2); 3.37 (m, 49H, 12- CH_3); 2.45-2.16 (m, 32H, 5- CH + 14- CH); 2.00-1.28 (m, 136H, 4- CH_2 + 13- CH_2 + 16- CH_2 + 17- CH_2); 1.16-1.06 (m, 12H, 2- CH_3 + 3- CH_3); 0.93 (m, 48H, 18- CH_3) ppm.

P2: 4.26-3.92 (m, 296H, 1- CH_2 + 6- CH_2 + 15- CH_2); 3.69-3.58 (m, 2253H, 7- CH_2 + 8- CH_2 + 9- CH_2 + 10- CH_2); 3.56-3.51 (m, 166H, 11- CH_2); 3.37 (m, 232H, 12- CH_3); 2.45-2.16 (m, 149H, 5- CH + 14- CH); 2.00-1.28 (m, 664H, 4- CH_2 + 13- CH_2 + 16- CH_2 + 17- CH_2); 1.16-1.06 (m, 12H, 2- CH_3 + 3- CH_3); 0.93 (m, 229H, 18- CH_3) ppm.

P3: 4.26-3.92 (m, 614H, 1-CH₂ + 6-CH₂ + 15-CH₂); 3.69-3.58 (m, 4565H, 7-CH₂ + 8-CH₂ + 9-CH₂ + 10-CH₂); 3.56-3.51 (m, 332H, 11-CH₂); 3.37 (m, 467H, 12-CH₃); 2.45-2.16 (m, 291H, 5-CH + 14-CH); 2.00-1.28 (m, 1373H, 4-CH₂ + 13-CH₂ + 16-CH₂ + 17-CH₂); 1.16-1.06 (m, 12H, 2-CH₃ + 3-CH₃); 0.93 (m, 462H, 18-CH₃) ppm.

P4: 4.26-3.92 (m, 2348H, 1-CH₂ + 6-CH₂ + 15-CH₂); 3.69-3.58 (m, 17503H, 7-CH₂ + 8-CH₂ + 9-CH₂ + 10-CH₂); 3.56-3.51 (m, 1249H, 11-CH₂); 3.37 (m, 1770H, 12-CH₃); 2.45-2.16 (m, 1148H, 5-CH + 14-CH); 2.00-1.28 (m, 5372H, 4-CH₂ + 13-CH₂ + 16-CH₂ + 17-CH₂); 1.16-1.06 (m, 12H, 2-CH₃ + 3-CH₃); 0.93 (m, 1808H, 18-CH₃) ppm.

P5: 4.26-3.92 (m, 3909H, 1-CH₂ + 6-CH₂ + 15-CH₂); 3.69-3.58 (m, 28902H, 7-CH₂ + 8-CH₂ + 9-CH₂ + 10-CH₂); 3.56-3.51 (m, 2056H, 11-CH₂); 3.37 (m, 2901H, 12-CH₃); 2.45-2.16 (m, 1904H, 5-CH + 14-CH); 2.00-1.28 (m, 8873H, 4-CH₂ + 13-CH₂ + 16-CH₂ + 17-CH₂); 1.16-1.06 (m, 12H, 2-CH₃ + 3-CH₃); 0.93 (m, 3033H, 18-CH₃) ppm.

P6: 4.26-3.92 (m, 4510H, 1-CH₂ + 6-CH₂ + 15-CH₂); 3.69-3.58 (m, 26150H, 7-CH₂ + 8-CH₂ + 9-CH₂ + 10-CH₂); 3.56-3.51 (m, 1880H, 11-CH₂); 3.37 (m, 2634H, 12-CH₃); 2.45-2.16 (m, 2228H, 5-CH + 14-CH); 2.00-1.28 (m, 9945H, 4-CH₂ + 13-CH₂ + 16-CH₂ + 17-CH₂); 1.16-1.06 (m, 12H, 2-CH₃ + 3-CH₃); 0.93 (m, 4217H, 18-CH₃) ppm.

P7: 4.26-3.92 (m, 5368H, 1-CH₂ + 6-CH₂ + 15-CH₂); 3.69-3.58 (m, 22574H, 7-CH₂ + 8-CH₂ + 9-CH₂ + 10-CH₂); 3.56-3.51 (m, 1881H, 11-CH₂); 3.37 (m, 2360H, 12-CH₃); 2.45-2.16 (m, 2638H, 5-CH + 14-CH); 2.00-1.28 (m, 12962H, 4-CH₂ + 13-CH₂ + 16-CH₂ + 17-CH₂); 1.16-1.06 (m, 12H, 2-CH₃ + 3-CH₃); 0.93 (m, 5797H, 18-CH₃) ppm.

P8: 4.26-3.92 (m, 5374H, 1-CH₂ + 6-CH₂ + 15-CH₂); 3.69-3.58 (m, 22525H, 7-CH₂ + 8-CH₂ + 9-CH₂ + 10-CH₂); 3.56-3.51 (m, 1619H, 11-CH₂); 3.37 (m, 2297H, 12-CH₃); 2.45-2.16 (m, 2746H, 5-CH + 14-CH); 2.00-1.28 (m, 13276H, 4-CH₂ + 13-CH₂ + 16-CH₂ + 17-CH₂); 1.16-1.06 (m, 12H, 2-CH₃ + 3-CH₃); 0.93 (m, 6102H, 18-CH₃) ppm.

P9: 4.26-3.92 (m, 5686H, 1-CH₂ + 6-CH₂ + 15-CH₂); 3.69-3.58 (m, 21521H, 7-CH₂ + 8-CH₂ + 9-CH₂ + 10-CH₂); 3.56-3.51 (m, 1525H, 11-CH₂); 3.37 (m, 2194H, 12-CH₃); 2.45-2.16 (m, 2816H, 5-CH + 14-CH); 2.00-1.28 (m, 13909H, 4-CH₂ + 13-CH₂ + 16-CH₂ + 17-CH₂); 1.16-1.06 (m, 12H, 2-CH₃ + 3-CH₃); 0.93 (m, 6398H, 18-CH₃) ppm.

P10: 4.26-3.92 (m, 5898H, 1-CH₂ + 6-CH₂ + 15-CH₂); 3.69-3.58 (m, 20887H, 7-CH₂ + 8-CH₂ + 9-CH₂ + 10-CH₂); 3.56-3.51 (m, 1499H, 11-CH₂); 3.37 (m, 2129H, 12-CH₃); 2.45-2.16 (m, 2939H, 5-CH + 14-CH); 2.00-1.28 (m, 14796H, 4-CH₂ + 13-CH₂ + 16-CH₂ + 17-CH₂); 1.16-1.06 (m, 12H, 2-CH₃ + 3-CH₃); 0.93 (m, 7068H, 18-CH₃) ppm.

P11: 4.26-3.92 (m, 6108H, 1-CH₂ + 6-CH₂ + 15-CH₂); 3.69-3.58 (m, 20090H, 7-CH₂ + 8-CH₂ + 9-CH₂ + 10-CH₂); 3.56-3.51 (m, 1450H, 11-CH₂); 3.37 (m, 2054H, 12-CH₃); 2.45-2.16 (m, 3024H, 5-CH + 14-CH); 2.00-1.28 (m, 15848H, 4-CH₂ + 13-CH₂ + 16-CH₂ + 17-CH₂); 1.16-1.06 (m, 12H, 2-CH₃ + 3-CH₃); 0.93 (m, 7402H, 18-CH₃) ppm.

P12: 4.26-3.92 (m, 6768H, 1-CH₂ + 6-CH₂ + 15-CH₂); 3.69-3.58 (m, 18536H, 7-CH₂ + 8-CH₂ + 9-CH₂ + 10-CH₂); 3.56-3.51 (m, 1856H, 11-CH₂); 3.37 (m, 2005H, 12-CH₃); 2.45-2.16 (m, 3267H, 5-CH + 14-CH); 2.00-1.28 (m, 17298H, 4-CH₂ + 13-CH₂ + 16-CH₂ + 17-CH₂); 1.16-1.06 (m, 12H, 2-CH₃ + 3-CH₃); 0.93 (m, 7924H, 18-CH₃) ppm.

2.3 Determination of monomer conversion from ¹H NMR spectra

Samples were drawn from the P(OEGA-co-BA) reaction mixture and quenched to determine the conversion of the polymerisations time-dependently by ¹H NMR from the crude mixture. For quantification, the ratio of the reacted to unreacted monomer was determined. Therefore, the intensities of the methyl groups of both monomers and the polymer at $\delta = 3.35$ and 0.91 ppm (indicated in dark blue/brown in Fig. S2) were collectively normalised to 300% and referenced to the three vinyl multiplets of the unreacted monomers at $\delta = 6.5$ -5.5 ppm (indicated in light blue/brown in Fig. S2). Each integral I_1 - I_3 of the multiplets corresponding to the three protons of the vinyl group indicates the remaining percentage of unreacted monomer

in the mixture. The overall conversion p was determined by averaging the three calculated intensities I_1 , I_2 , I_3 of the vinyl protons according to the following equation.

$$p = 100\% - \left(\frac{I_1 + I_2 + I_3}{3} \right) \quad (\text{S1})$$

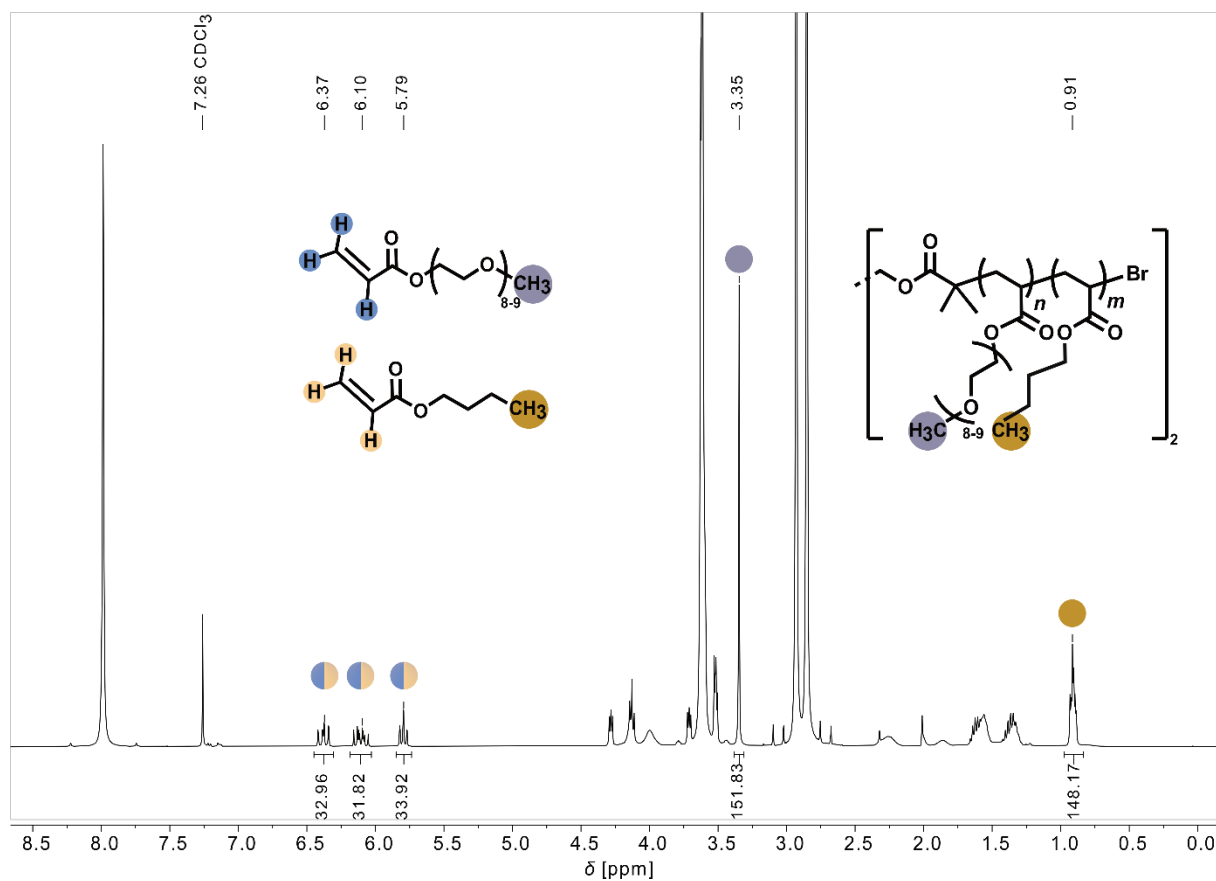


Figure S2. Representative ^1H NMR spectrum of the crude reaction mixture of **P5** with a targeted comonomer ratio of 1:1 in CDCl_3 after a reaction time of 6 h. Monomer and polymer signals, which have been used to calculate monomer conversion, are indicated with colour in the spectrum and the corresponding chemical structures.

2.4 Change in refractive index with copolymer concentration

Table S2. dn/dc values for copolymers **P2-P12** for GPC-MALS analysis in THF and water at 25 °C.

polymer	$dn\ dc^{-1}$ (THF) $[10^{-3}\ mL\ g^{-1}]$	$dn\ dc^{-1}$ (water) $[10^{-3}\ mL\ g^{-1}]$
P2	67.6 ± 0.3	127.0 ± 0.2
P3	68.6 ± 0.2	132.0 ± 0.2
P4	69.8 ± 0.2	132.0 ± 0.1
P5	69.3 ± 0.4	133.1 ± 0.3
P6	70.6 ± 0.4	130.0 ± 0.1
P7	66.8 ± 0.1	129.0 ± 0.1
P8	65.2 ± 0.1	128.0 ± 0.4
P9	65.8 ± 0.1	128.0 ± 0.2
P10	65.5 ± 0.3	128.0 ± 0.2
P11	66.6 ± 0.2	n.d. ^a
P12	69.4 ± 0.4	n.d. ^a

^a n.d. = not determined due to low T_{CP} in water.

2.5 Optimisation of copolymerisation parameters

Table S3. Monomer conversion p (%) after 6 h statistical copolymerisation of BA and OEGA at 25 °C as determined by ^1H NMR spectroscopy of the crude reaction mixture testing various catalyst concentrations. ($N \geq 2$)

polymer	OEGA [mmol]	BA [mmol]	2f-BiB [μmol]	CuBr ₂ [μmol]	Me ₆ TREN [μmol]	[OEGA+BA]/DMF [v/v]	p [%]
P1	16.4	16.4	1037.3	5.2	18.7	1/1	98.7 \pm 0.4
				16.6	60.2		98.5 \pm 0.2
				29.0	104.8		98.6 \pm 0.3
				40.5	145.8		97.7 \pm 0.8
				51.9	186.7		92.5 \pm 1.8
P2	16.4	16.4	201.5	1.0	3.6	1/1	92.5 \pm 1.4
				3.2	11.7		96.3 \pm 0.5
				5.6	20.3		95.1 \pm 1.1
				7.9	28.2		95.2 \pm 0.7
				10.1	36.3		94.4 \pm 1.2
P3	16.4	16.4	100.4	32.8	118.3	1/1	77.2 \pm 0.7
				1.6	5.8		83.2 \pm 2.3
				2.8	10.1		90.7 \pm 0.4
				3.9	14.1		90.8 \pm 1.3
				5.0	18.1		90.0 \pm 0.2
P4	16.4	16.4	20.0	16.4	58.9	1/1	86.8 \pm 0.3
				27.6	99.4		85.0 \pm 0.3
				0.6	2.0		68.8 \pm 0.2
				0.8	2.8		76.7 \pm 0.5
				1.0	3.6		73.1 \pm 1.5
P5	16.4	16.4	10.0	3.3	11.7	1/1	68.7 \pm 1.1
				5.5	19.8		66.4 \pm 0.8
				0.3	1.0		59.2 \pm 0.7
				0.4	1.4		68.5 \pm 1.9
				0.5	1.8		67.6 \pm 0.3
				1.6	5.9		63.6 \pm 2.8
				2.8	9.9		49.6 \pm 2.6

3. Kinetics of the copolymerisation of OEGA and BA

3.1 Controlled copolymerisation

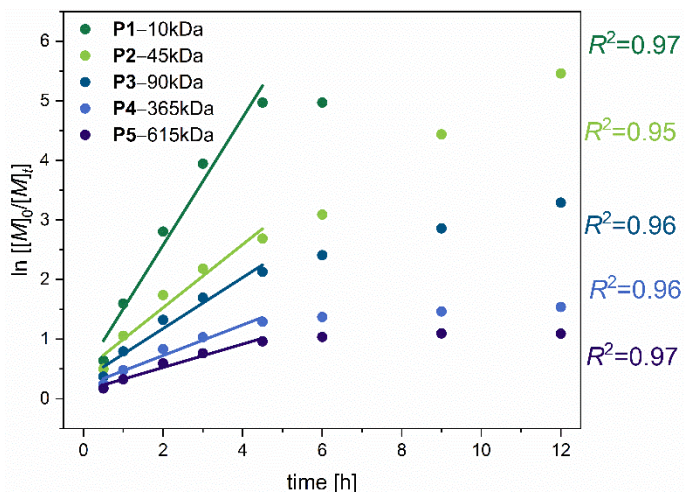


Figure S3. Kinetic plot of $\ln [M]_0/[M]_t$ versus reaction time for the copolymerisation of OEGA with BA at 25 °C to yield **P1-P5** with a comonomer ratio of 1:1.

Table S4. Reaction conditions for the copolymerisation of OEGA with BA at 25 °C to determine the reactivity ratios via the Finemann-Ross and the extended Kelen-Tüdös approach.

OEGA:BA	M_n^a	OEGA [mmol]	BA [mmol]	2f-BiBr ₃ [μmol]	CuBr ₂ [μmol]	Me ₆ TREN [μmol]	[OEGA+BA]/DMF [v/v]
70:30	1000	18.7	8.0	10.0	0.5	1.8	1/1
60:40	1000	17.7	11.8	10.0	0.5	1.8	1/1
50:50	1000	16.4	16.4	10.0	0.5	1.8	1/1
40:60	1000	14.9	22.3	10.0	0.5	1.8	1/1
30:70	1000	12.8	30.0	10.0	0.5	1.8	1/1

^a targeted molecular weight.

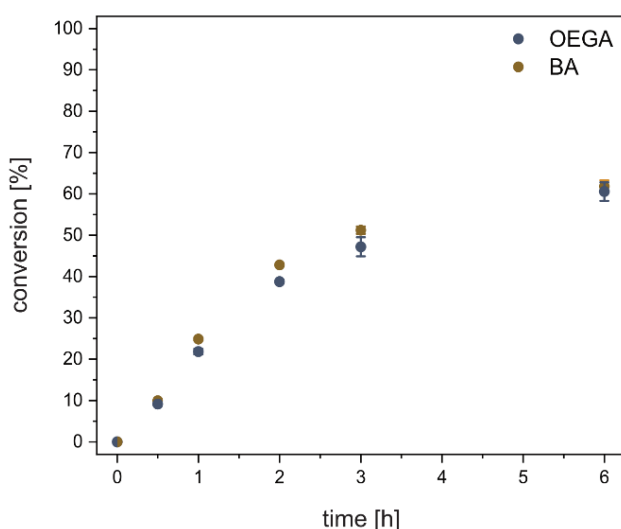
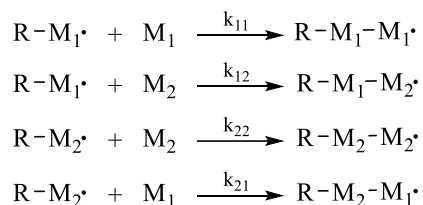


Figure S4. Time-dependent monomer conversion during statistical copolymerisation to yield **P5** with a fixed 1:1 comonomer ratio via ARGET ATRP in DMF at 25 °C. ($N = 2$)

3.2 Determination of the reactivity ratios by the Fineman-Ross approach^[2-4]

The copolymerisation of two monomers, M_1 and M_2 , can be described by the growth steps listed in Scheme S1.



Scheme S1. Possible growth steps of a binary copolymerisation of the monomers M_1 and M_2 .^[4]

Assuming that the comonomer conversion drift is negligible at low conversions (< 10%), the copolymer composition equation – considering only the effect of the terminal unit – is defined in equation (S2), where M_1 refers to OEGA and M_2 refers to BA. In this context, r_1 and r_2 represent the respective copolymerisation parameters. M_1 and M_2 denote the molar concentrations of the monomers in the feedstock, while m_1 and m_2 represent the molar concentrations of the monomers in the copolymer.

$$\frac{dM_1}{dM_2} = \frac{M_1}{M_2} \cdot \frac{r_1 M_1 + M_2}{r_2 M_2 + M_1} = \frac{m_1}{m_2} \quad (\text{S2})$$

$$r_1 = \frac{k_{11}}{k_{12}} \quad (\text{S3})$$

$$r_2 = \frac{k_{22}}{k_{21}} \quad (\text{S4})$$

Equation S2 can then be simplified to equation S7 by using S5 and S6.

$$f = \frac{M_1}{M_2} \quad (\text{S5})$$

$$F = \frac{m_1}{m_2} \quad (\text{S6})$$

$$F = f \frac{1 + r_1 f}{r_2 + f} \quad (\text{S7})$$

By further rearranging the terms and simplifying using equations S8 and S10, the linearised Fineman-Ross equation (S10) is obtained, from which the copolymerisation parameters can be determined from the slope ($-r_2$) and the intercept (r_1).

$$G = \frac{f(F-1)}{F} \quad (\text{S8})$$

$$H = \frac{f^2}{F} \quad (\text{S9})$$

$$G = r_1 H - r_2 \quad (\text{S10})$$

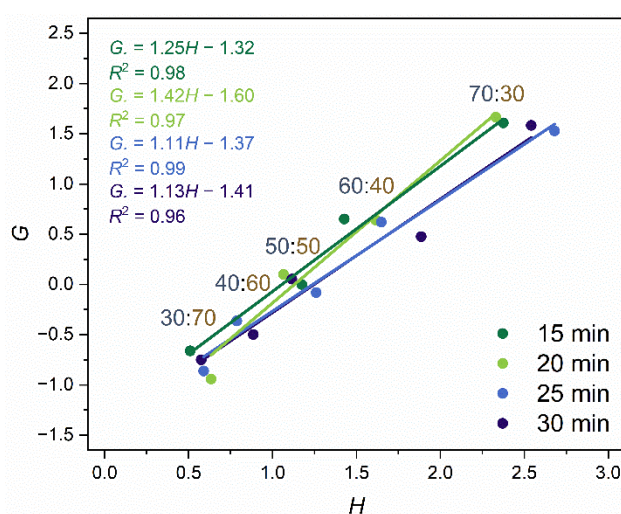


Figure S5. Fineman-Ross plot for the copolymerisation with feed ratios of OEGA:BA = 30:70 - 70:30 in increments of 10 mol% aiming at an $M_n = 1000$ kDa.

3.3 Determination of the reactivity ratios by the extended Kelen-Tüdös approach^[3,5,6]

A requirement of Fineman-Ross plots is a low conversion $< 10\%$ to ensure that the assumption of negligible concentration drifts due to comonomer conversion is valid,^[2,5] which is fulfilled for the studied copolymerisation within the first 30 minutes of the polymerisations under the optimised conditions. However, the obtained data is asymmetric, resulting in different r_1 and r_2 values when the attribution of the monomers as M_1 and M_2 is switched.^[2,5] To reduce such arbitrary effects, the Kelen-Tüdös approach was introduced with an arbitrary factor α (S11) yielding more uniformly distributed experimental data points between $\xi = 0-1$.^[2,5]

$$\alpha = (H_{\max} \cdot H_{\min})^{0.5} \quad (\text{S11})$$

The linearised copolymerisation equation, according to Kelen-Tüdös is defined as S12, with the relationship to the Fineman-Ross equation established through equations S13 and S14.

$$\eta = \left(r_1 + \frac{r_2}{\alpha}\right)\xi - \frac{r_2}{\alpha} \quad (\text{S12})$$

$$\eta = \frac{G}{\alpha + H} \quad (\text{S13})$$

$$\xi = \frac{H}{\alpha + H} \quad (\text{S14})$$

The extended Kelen-Tüdös approach additionally considers effects of advancing conversion and thus becomes applicable even at higher conversion levels than 10%.^[2,5] The partial molar conversion ζ_2 of M_2 is defined by equation S15, where W represents the weight conversion during polymerisation, and μ is the ratio of the molecular weight of M_2 to that of M_1 . Similarly, the partial molar conversion ζ_1 of M_1 is given by equation S16.

$$\zeta_2 = W \frac{\mu + f}{\mu + F} \quad (\text{S15})$$

$$\zeta_1 = \frac{\zeta_2 F}{f} \quad (\text{S16})$$

Subsequently, the conversion-dependent parameter Z is defined as follows:

$$Z = \frac{\log(1 - \zeta_1)}{\log(1 - \zeta_2)} \quad (\text{S17})$$

Consequently, the previous parameters can be redefined in the following manner:

$$H = \frac{F}{Z^2} \quad (\text{S18})$$

$$G = \frac{F - 1}{Z} \quad (\text{S19})$$

$$\eta = \frac{G}{\alpha + H} \quad (\text{S20})$$

$$\xi = \frac{H}{\alpha + H} \quad (\text{S21})$$

By plotting η against ξ , the copolymerisation parameters r_1 and r_2 can finally be determined as follows:

$$\xi(0) = -\frac{r_2}{\alpha} \quad (\text{S22})$$

$$\xi(1) = r_1 \quad (\text{S23})$$

4. GPC traces in tetrahydrofuran and water

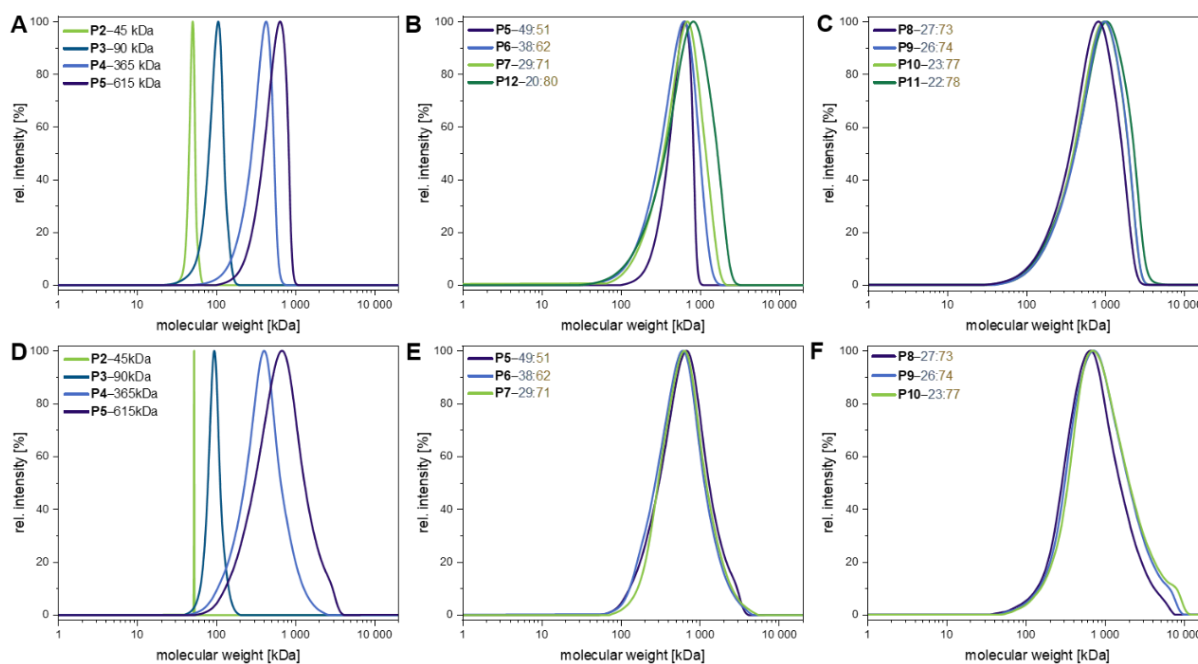


Figure S6. Representative GPC traces of (A) **P2-P5** with a fixed 1:1 comonomer ratio and varying molecular weight, (B) **P5-P7**, **P12** and (C) **P8-P11** with a fixed molecular weight of around 600 kDa and varying OEGA:BA ratios in THF detected with an RI and MALS detector at 25 °C, as well as (D) **P2-P5** with a fixed 1:1 comonomer ratio and varying molecular weight, (E) **P5-P7** and (F) **P8-P10** with a fixed molecular weight of around 600 kDa and varying OEGA:BA ratios in water detected with an RI and MALS detector at 25 °C.

5. Optimisation of the copolymer purification process

As a potential candidate for biomedical applications, such as drug delivery, it is essential to eliminate the cytotoxic copper content and effectively purify the crude polymer to remove reaction residues. Therefore, several purification methods – based on filtration, extraction, and dialysis – were compared. Residual copper traces were quantified using atomic absorption spectroscopy, while the amount of reaction residues was determined via ^1H NMR spectroscopy. For purification via filtration, DMF was first removed under high vacuum, the crude product (10 g) was dissolved in THF (100 mL) and subsequently filtered through neutral (**F1**) and basic alumina columns (**F2**) (Table S5). Both filtration methods resulted in a 75% reduction in the residual copper concentration. Alternatively, copper removal from the concentrated crude reaction mixture was attempted through liquid-liquid extraction (**E**). After solvent removal, the crude product (10 g) was dissolved in dichloromethane (100 mL) and extracted with a 1 M NH_4Cl solution (3x100 mL), yielding an overall copper reduction of 67% relative to the crude product (**N**). However, a major drawback of both methods was the incomplete removal of unreacted monomers from the product (Fig. S7). To simplify the purification process and avoid multiple steps, dialysis was considered as an alternative method, with various media and differing numbers of cycles (**D1-D7**). Generally, dialysis was first conducted in water to remove water-soluble catalysts, unreacted OEGA, and DMF, followed by ethanol to extract the hydrophobic BA. Since the copper was already complexed with Me_6TREN , using a 1 mM EDTA solution (**D1**, 78% removal) did not improve copper removal compared to pure water (**D2**, 82% removal) as the dialysis medium. The effectiveness of copper removal decreased as the number of dialysis cycles was reduced, both in water (82% in **D2** vs. 67% in **D3**) and ethanol (82% in **D2** vs. 72% in **D4** vs 67% in **D5**). Switching from ethanol (**D5**, 67% removal) to methanol (**D6**, 67% removal) as the dialysis medium had no additional effect on the residual copper levels. When dialysis was performed exclusively in ethanol (**D7**, 76% removal), copper concentrations were slightly higher compared to **D2** (82% removal), likely due to the reduced total dialysis volume and

fewer cycles, which also hindered the complete removal of unreacted monomers from the solution (Fig. S7). Based on these results, dialysis **D2** was the most effective purification method, achieving an 82% reduction in copper content and complete removal of unreacted monomers. This was exemplified by polymer **P5**, which exhibited a residual copper concentration of approximately 2.4 ppm.

Table S5. Residual copper concentration in the final polymer **P5** as determined by AAS after applying different purification protocols on 10 g of the crude product. ($n = 7$)

Purification technique		Copper concentration [ppm]
No purification	N	13.5 ± 0.1
Filtration	F1 neutral alumina column	3.4 ± 0.1
	F2 basic alumina column	3.3 ± 0.1
Extraction	E 3 x 1 M NH ₄ Cl / DCM	4.5 ± 0.1
Dialysis [MWCO 3.5 kDa]	D1 3 x 2 L 1 mM EDTA 3 x 2 L H ₂ O 3 x 1 L EtOH	3.0 ± 0.1
	D2 6 x 2 L H ₂ O 3 x 1 L EtOH	2.4 ± 0.1
	D3 3 x 2 L H ₂ O 3 x 1 L EtOH	4.4 ± 0.1
	D4 6 x 2 L H ₂ O 2 x 1 L EtOH	3.8 ± 0.1
	D5 6 x 2 L H ₂ O 1 x 1 L EtOH	4.5 ± 0.1
	D6 6 x 2 L H ₂ O 1 x 1 L MeOH	4.5 ± 0.1
	D7 6 x 1 L EtOH	3.2 ± 0.1

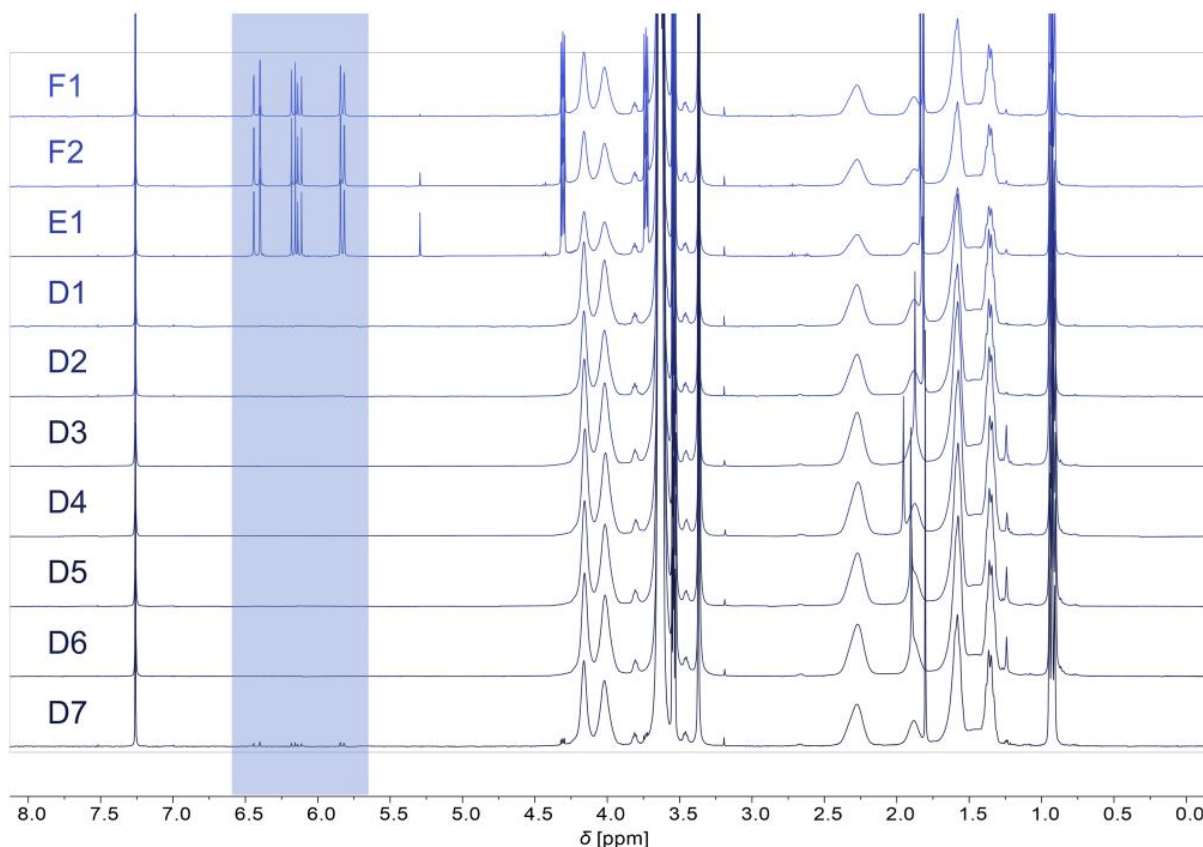


Figure S7. ^1H NMR spectra of differently purified batches of copolymer **P5** indicating its efficiency according to the residual monomer concentration within the polymer. Abbreviation code for the purification method as stated in **Table S5**.

6. Cell compatibility testing of P(OEGA-co-BA)

Adherent Caco-2 cells were exposed to polymer **P5** dissolved in cell culture medium for 24 and 48 h before the MTT reagent was added. Cell viability was assessed via the metabolic activity quantified by the colour change of the metabolised MTT reagent (Fig. S8). A non-significant change in the cells' metabolic activity was detected after 24 and 48 h exposure up to a polymer concentration of 1 mg mL^{-1} . Only at comparably high local concentrations for administration of 10 mg mL^{-1} a reduced activity of $\sim 70\%$ was observed, which, according to the DIN EN ISO 10993 for the biological assessment of medical products, is still acceptable.^[7]

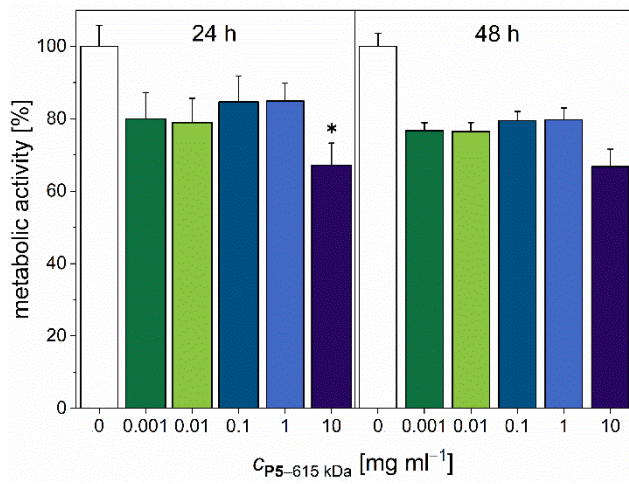


Figure S8. Metabolic activity of Caco-2 cells after treatment with polymer **P5** at varying concentrations for 24 and 48 h assessed via an MTT assay. ($N = 3$) Statistical significance ($p < 0,05$) as determined via a Kruskal-Wallis-ANOVA test is indicated with *.

7. Micelle formation in water evidenced by ^1H NMR spectroscopy

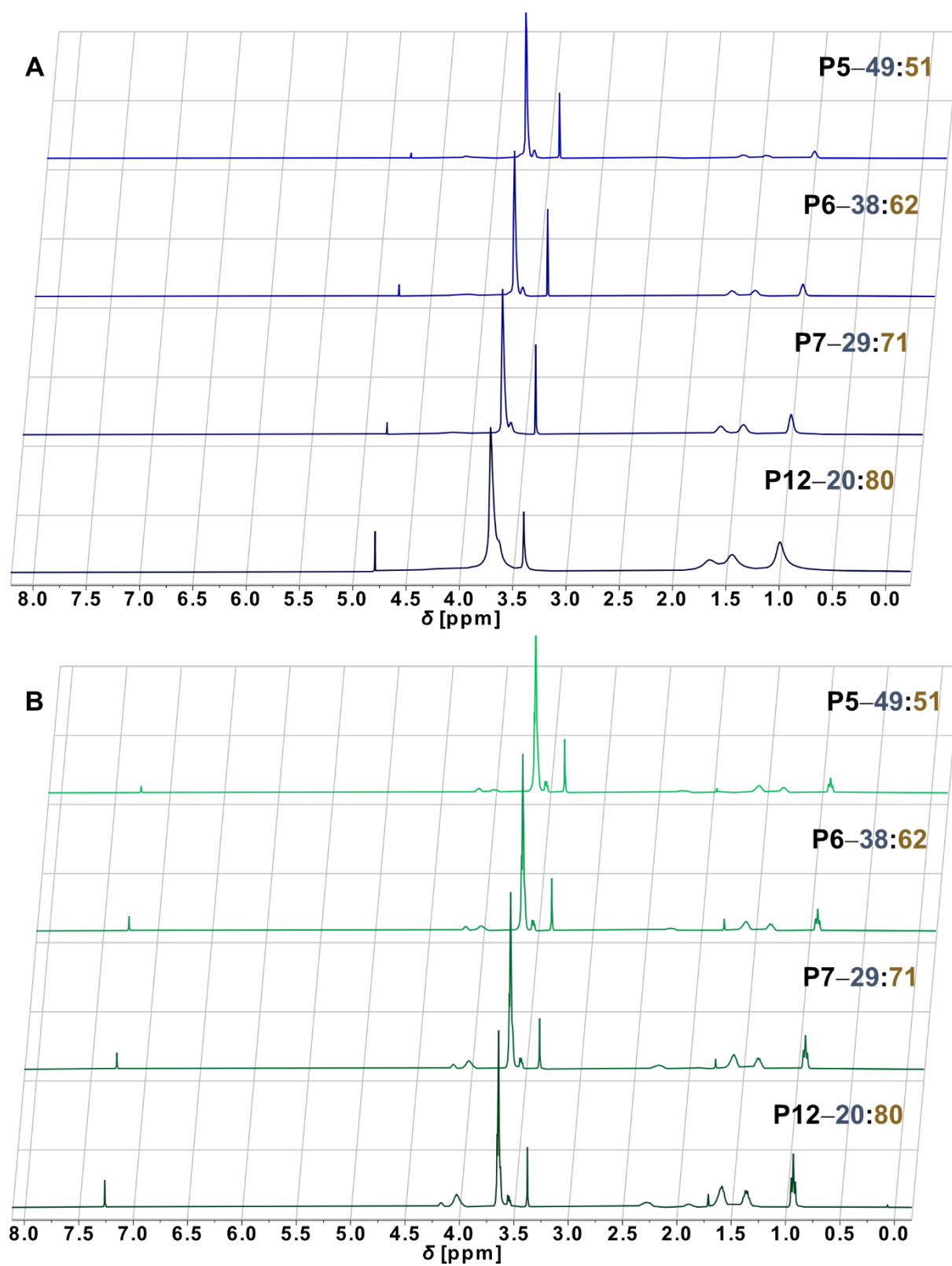


Figure S9. Representative ^1H NMR spectra of P5-P7 and P12 in (A) D_2O and (B) CDCl_3 .

^1H NMR spectra of statistical P(OEGA-*co*-BA) copolymers **P5-P7** and **P12** recorded in D_2O and CDCl_3 are shown in **Figure S9**. The peak integrals were referenced to the three protons of the terminal methoxy groups of the OEGA-based units located at around 3.4 ppm, which are expected to be well-solvated in CDCl_3 and D_2O . Ratios of distinct proton signal intensities in spectra recorded in D_2O and CDCl_3 were calculated (**Table S6**). Particularly, proton signal intensities in D_2O attributed to methylene groups near the polymer backbone ($\delta = 1.25\text{-}2.80$ and $\delta = 3.48\text{-}4.55$) are significantly decreased compared to the respective signals in CDCl_3 .

Table S6. Ratio of distinct proton signal intensities $I_{\text{D}_2\text{O}}/I_{\text{CDCl}_3}$ in ^1H NMR spectra of statistical P(OEGA-*co*-BA) copolymers **P5-P7** and **P12** recorded in CDCl_3 and D_2O at room temperature.

polymer	composition ^a [OEGA:BA]	composition ^b [OEGA:BA]	$I_{\text{D}_2\text{O}}/I_{\text{CDCl}_3}$ (0.60-1.25 ppm)	$I_{\text{D}_2\text{O}}/I_{\text{CDCl}_3}$ (1.25-2.80 ppm)	$I_{\text{D}_2\text{O}}/I_{\text{CDCl}_3}$ (3.30-3.48 ppm)	$I_{\text{D}_2\text{O}}/I_{\text{CDCl}_3}$ (3.48-4.55 ppm)
P5	49:51	50:50	0.97	0.91	1.00	0.98
P6	38:62	38:62	1.03	0.91	1.00	1.00
P7	29:71	29:71	0.97	0.77	1.00	0.90
P12	20:80	22:78	0.91	0.51	1.00	0.66

^a molar ratio determined in CDCl_3 , ^b molar ratio determined in D_2O .

8. Determination of the copolymers' association number in water^[8,9]

The association behaviour of the polymers in water was assessed by comparing the molecular weights obtained from GPC-MALS measurements in THF with those determined in water (eq. S24). This comparison allowed the determination of the polymer association number, providing insight into their aggregation behaviour in aqueous solution. It was assumed that association numbers around one correspond to unimolecular micelles, while values greater than one indicate the presence of multimolecular aggregates.

$$A_{\text{H}_2\text{O}} = M_{\text{n,H}_2\text{O}} M_{\text{n,THF}}^{-1} \quad (\text{S24})$$

9. Dynamic light scattering (DLS) measurements during dilution

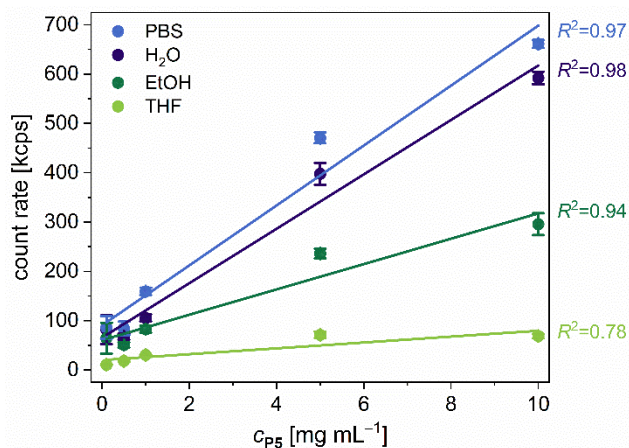


Figure S10. Dependence of light scattering intensity on concentration for **P5** in different media at 25 °C measured at a fixed incident light intensity. ($n = 3$)

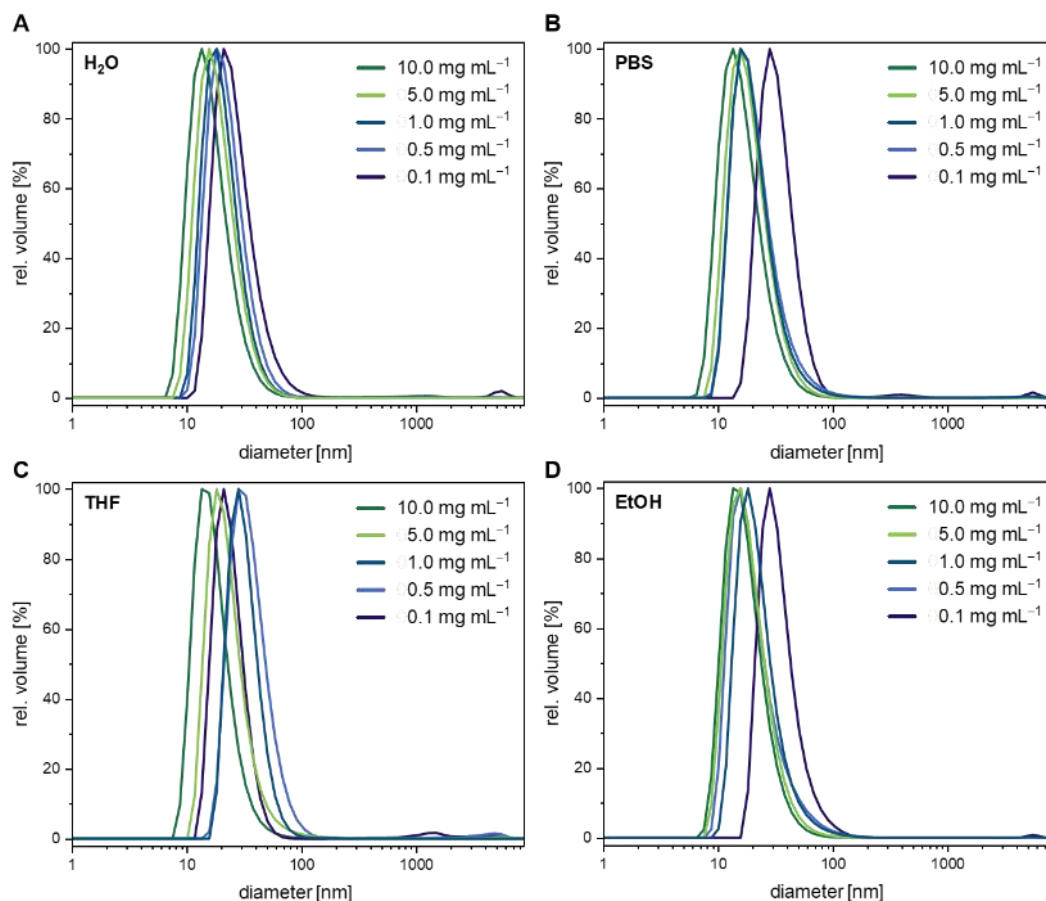


Figure S11. Representative DLS curves of **P5** during dilution in different media: (A) water, (B) PBS, (C) THF, and (D) EtOH at 25 °C measured at a fixed incident light intensity. ($n = 3$)

Table S7. Hydrodynamic radii R_h of **P5** determined via DLS during dilution in different media at 25 °C at a fixed incident light intensity. ($n = 3$)

C_{P5} [mg mL ⁻¹]	$R_h^{H_2O}$ [nm]	R_h^{PBS} [nm]	R_h^{THF} [nm]	R_h^{EtOH} [nm]
10.0	8.5 ± 3.9 ^a	8.7 ± 4.3 ^a	8.8 ± 4.4	8.7 ± 4.7
5.0	9.5 ± 4.4	9.8 ± 4.7	10.6 ± 7.3	9.5 ± 5.7
1.0	10.3 ± 4.8 ^a	9.9 ± 6.3 ^a	16.0 ± 7.1	12.4 ± 8.4
0.5	11.1 ± 5.6	10.9 ± 7.0	15.7 ± 7.8	10.7 ± 7.9
0.1	16.0 ± 7.7 ^{a,b}	16.9 ± 6.1 ^{a,b}	11.4 ± 7.9 ^b	18.2 ± 8.0 ^b

^a deviations from values stated in Figure 2A/Table 2 are due to the use of different devices or different measurement methods. ^b high inaccuracy due to too low scattering intensity.

10. Rheology of copolymers P(OEGA-co-BA) to determine their intrinsic viscosity

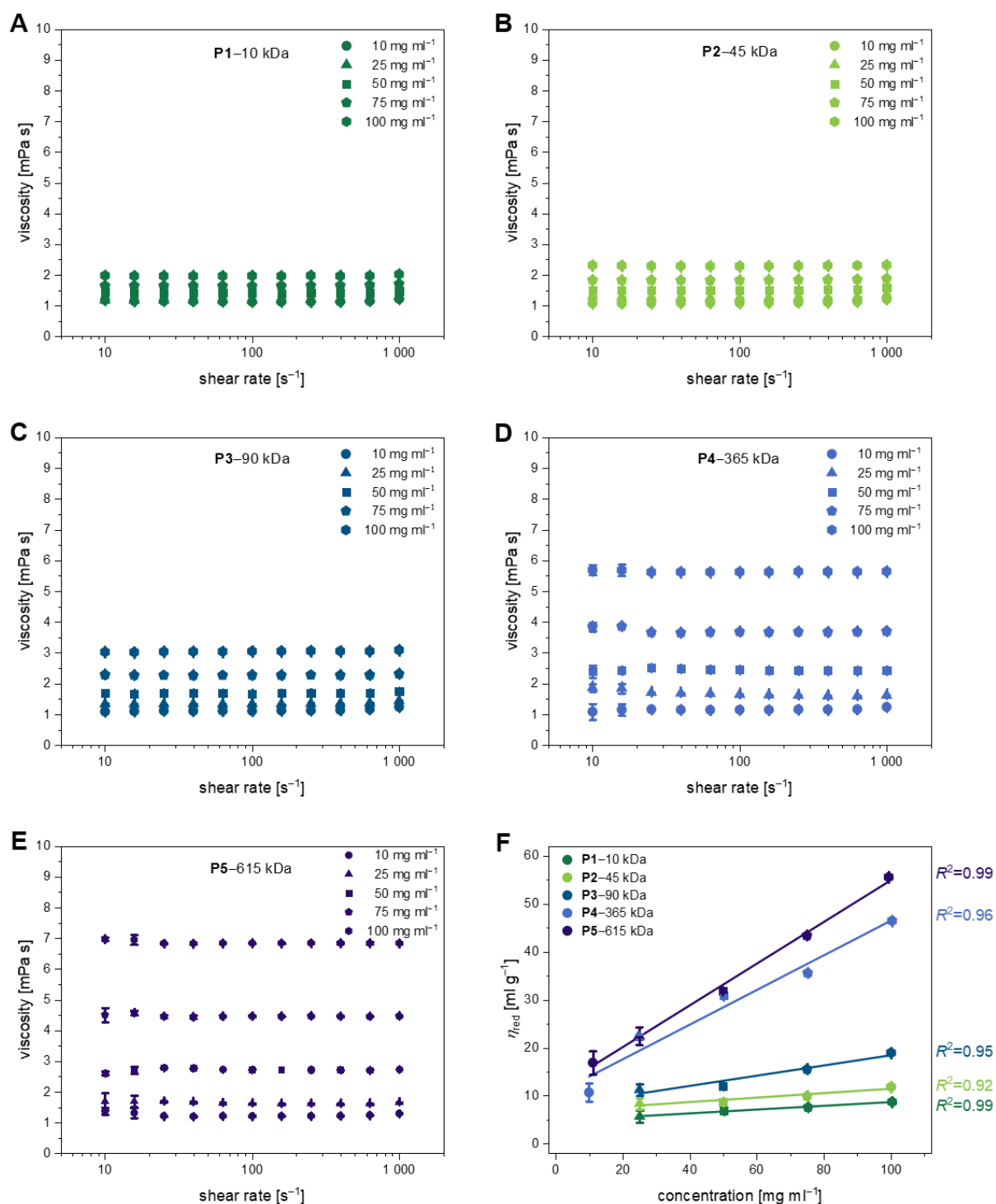


Figure S12. (A)-(E) Shear rate-dependent viscosity of aqueous copolymer solutions of **P1-P5** with increasing molecular weight measured on a plate-plate rheometer at 25 °C with varying polymer concentration. ($N = 3$) (F) Reduced viscosity as a function of concentration.

11. Turbidity measurements of copolymers

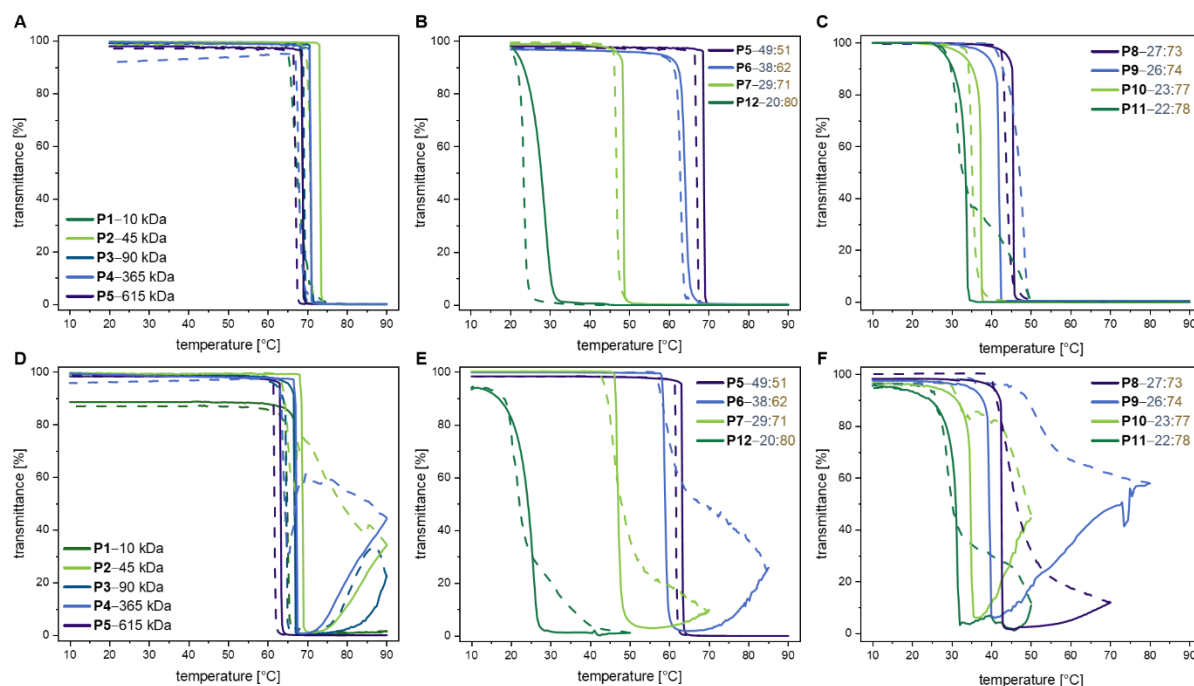


Figure S13. Representative turbidity curves of aqueous P(OEGA-co-BA) solutions as a function of temperature determined at heating (solid) and cooling (dashed) rates of 0.5 °C min^{-1} and a concentration of 10 mg ml^{-1} . Curves are grouped with respect to increasing molecular weight **P1-P5** and comonomer ratio **P5-P7**, **P12** or **P8-P11** in (A,B,C) water and (D,E,F) PBS. ($n = 3$)

12. DLS measurements of copolymers below and above their T_{cp}

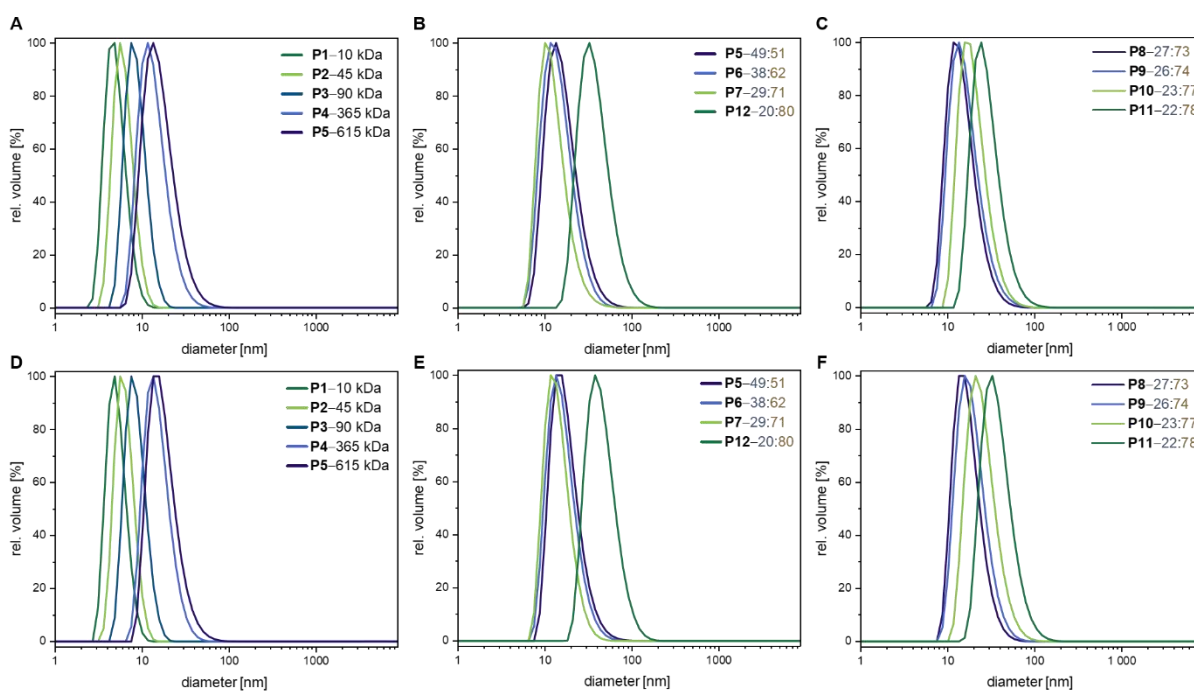


Figure S14. Representative DLS curves of P(OEGA-co-BA) copolymers (10 mg ml^{-1}) at 25 °C for **P1-P11** and at 20 °C for **P12**. Curves are grouped with respect to increasing molecular weight at a constant OEGA:BA = 1:1 ratio in (A) water and (D) PBS and varying ratio of OEGA:BA at a fixed molecular weight around 600 kDa in (B,C) water and (E,F) PBS. ($n = 3$)

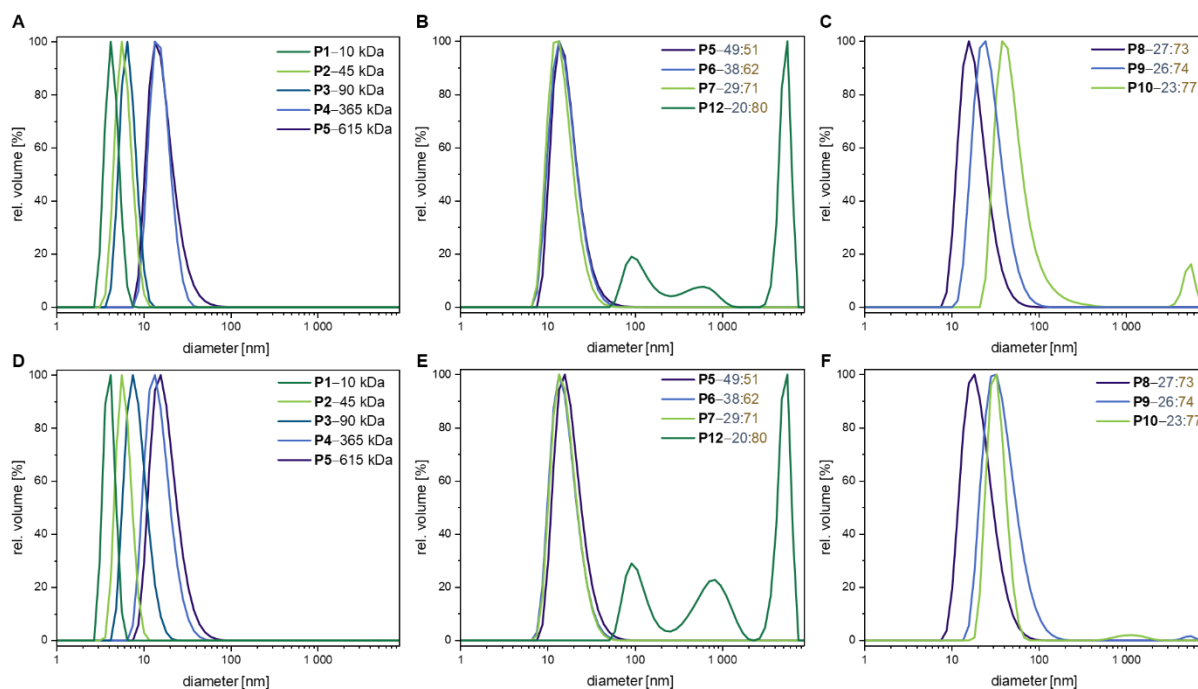


Figure S15. Representative DLS curves of P(OEGA-*co*-BA) copolymers **P1-P12** (10 mg ml⁻¹) at 37 °C. Curves are grouped with respect to increasing molecular weight at a constant OEGA:BA =1:1 ratio in (A) water and (D) PBS and varying ratio of OEGA:BA at a fixed molecular weight around 600 kDa in (B,C) water and (E,F) PBS. Of note, copolymer **P11** consistently produced unstable, large aggregates > 1 000 nm at TCP+10 °C, which were outside the detection range of the device. (*n* = 3)

Table S8. Hydrodynamic radii R_h of statistical P(OEGA-*co*-BA) copolymers **P1-P12** determined via DLS at a concentration of 10 mg ml⁻¹ below and above the T_{cp} in water and PBS. (*n* = 3)

polymer	composition ^a [OEGA:BA]	$R_h^{H_2O}$ (25 °C) [nm]	$R_h^{H_2O}$ ($T > T_{CP}$) ^b [nm]	R_h^{PBS} (25 °C) [nm]	R_h^{PBS} ($T > T_{CP}$) ^b [nm]
P1	49:51	2.5 ± 0.7	46.7 ± 15.2	2.6 ± 0.8	293.1 ± 67.4
P2	50:50	3.1 ± 0.9	35.5 ± 11.9	3.2 ± 1.0	151.5 ± 37.5
P3	49:51	4.3 ± 1.3	31.9 ± 10.2	4.3 ± 1.3	151.7 ± 44.8
P4	50:50	7.6 ± 3.0	29.0 ± 10.1	7.7 ± 3.0	130.9 ± 36.0
P5	50:50	8.3 ± 4.1	80.4 ± 22.7	8.9 ± 4.2	144.0 ± 33.6
P6	38:62	7.7 ± 3.6	43.5 ± 12.7	8.2 ± 3.5	150.0 ± 42.9
P7	29:71	7.2 ± 3.1	129.9 ± 38.2	7.4 ± 3.3	125.7 ± 36.1
P8	27:73	7.9 ± 3.6	95.4 ± 25.1	8.2 ± 3.6	88.0 ± 22.8
P9	26:74	8.8 ± 4.2	71.8 ± 17.6	9.5 ± 4.3	119.9 ± 32.8
P10	23:77	10.6 ± 4.5	157.5 ± 41.6	11.7 ± 6.1	244.7 ± 67.1
P11	22:78	14.7 ± 6.9	43.5 ± 9.2	19.2 ± 9.0	44.3 ± 11.7 2772.5 ± 67.1 ^d
P12	20:80	20.7 ± 9.4 ^c	50.0 ± 29.7 214.7 ± 117.3 ^d	24.6 ± 10.0 ^c	58.2 ± 56.2 2681.2 ± 352.7 ^d

^a molar ratio. ^b determined at $T = T_{CP} + 10$ °C. ^c determined by DLS at 20 °C. ^d bimodal distribution in DLS.

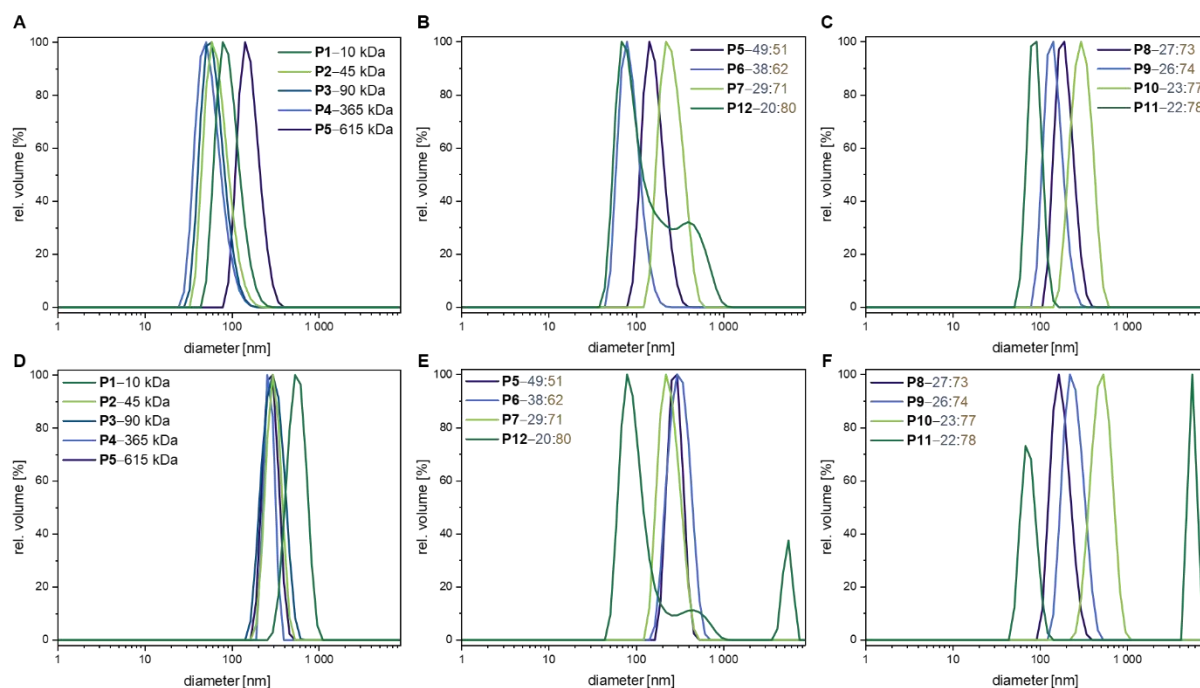


Figure S16. Representative DLS curves of P(OEGA-co-BA) copolymers **P1-P12** (10 mg mL⁻¹) at $T = T_{CP} + 10$ °C. Curves are grouped with respect to increasing molecular weight at a constant OEGA:BA = 1:1 ratio in (A) water and (D) PBS and varying ratio of OEGA:BA at a fixed molecular weight around 600 kDa in (B,C) water and (E,F) PBS. ($n = 3$)

13. Determination of maximum micelle loading capacity

To study the loading capacity of thermoresponsive P(OEGA-co-BA)-based micelles under physiological conditions, we used hydrophobic, UV-active pyrene as a model compound. Initially, the copolymers **P1-P12** (20 mg) were dissolved in 2 mL of a saturated methanol solution of pyrene. After dissolving the polymers, the methanol was removed under ultra-high vacuum (72 h). The remaining residue was then dissolved in D₂O (2 mL) for ¹H NMR analysis or in PBS (2 mL) for UV-Vis spectroscopy, resulting in a final polymer concentration of $c_{pol} = 10$ mg mL⁻¹. Excess of pyrene was removed by filtration through a cellulose acetate filter (0.45 μm). For the determination of pyrene concentration using UV-Vis spectroscopy, a calibration curve was prepared from pyrene solutions in pentane at defined concentrations of 2, 5, 10, 15, 20 μg mL⁻¹. Based on this calibration series, the pyrene concentration c_{pyr} in the sample solution was determined. The maximum absorbance intensity between 300-350 nm was then correlated with the amount of polymer in the solution. To calculate the ratio of pyrene molecules per polymer chain (N_{pyr}/N_{pol}), equation S25 was used along with the

molecular weight values of the polymers obtained from ^1H NMR measurements (Table 1).

$$\frac{N_{\text{pyr}}}{N_{\text{pol}}} = \frac{c_{\text{pyr}} M_{\text{pyr}}^{-1}}{c_{\text{pol}} M_{\text{pol}}^{-1}} \quad (\text{S25})$$

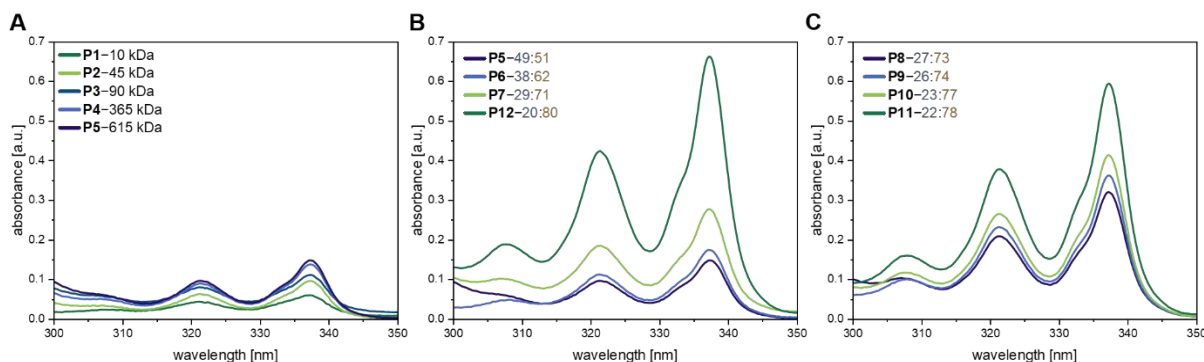


Figure S17. UV-Vis spectra of pyrene-loaded micelles at 10 mg mL^{-1} of (A) **P1-P5** with a fixed 1:1 comonomer ratio and (B) **P5-P7, P12**, (C) **P8-P11** with a fixed molecular weight around 600 kDa in PBS at 10°C for **P1-P12** to determine the amount of loaded pyrene within the micelles by comparison with a pyrene standard curve. Maximum micelle loading was accomplished with excess pyrene to derive the loading capacity. ($N = 2$)

To independently confirm the values obtained, the pyrene concentration per polymer was also determined using ^1H NMR spectroscopy. For this, the intensity of all pyrene proton signals at $\delta = 7.8\text{-}8.5$ (orange) were compared to the intensity of the methyl group signals from the polymer at $\delta = 3.35$ (OEGA, blue) and 0.91 ppm (BA, green) normalised to one polymer chain. This ratio was then converted into the number of pyrene molecules per polymer chain by considering the number of OEGA and BA repeating units per polymer, as follows:

$$\frac{N_{\text{pyr}}}{N_{\text{pol}}} = \frac{I_{\text{pyr}} \cdot 10^{-1}}{\left(\frac{I_{\text{CH}_3}}{N_{\text{OEGA}} + N_{\text{BA}}} \right)} \quad (\text{S26})$$

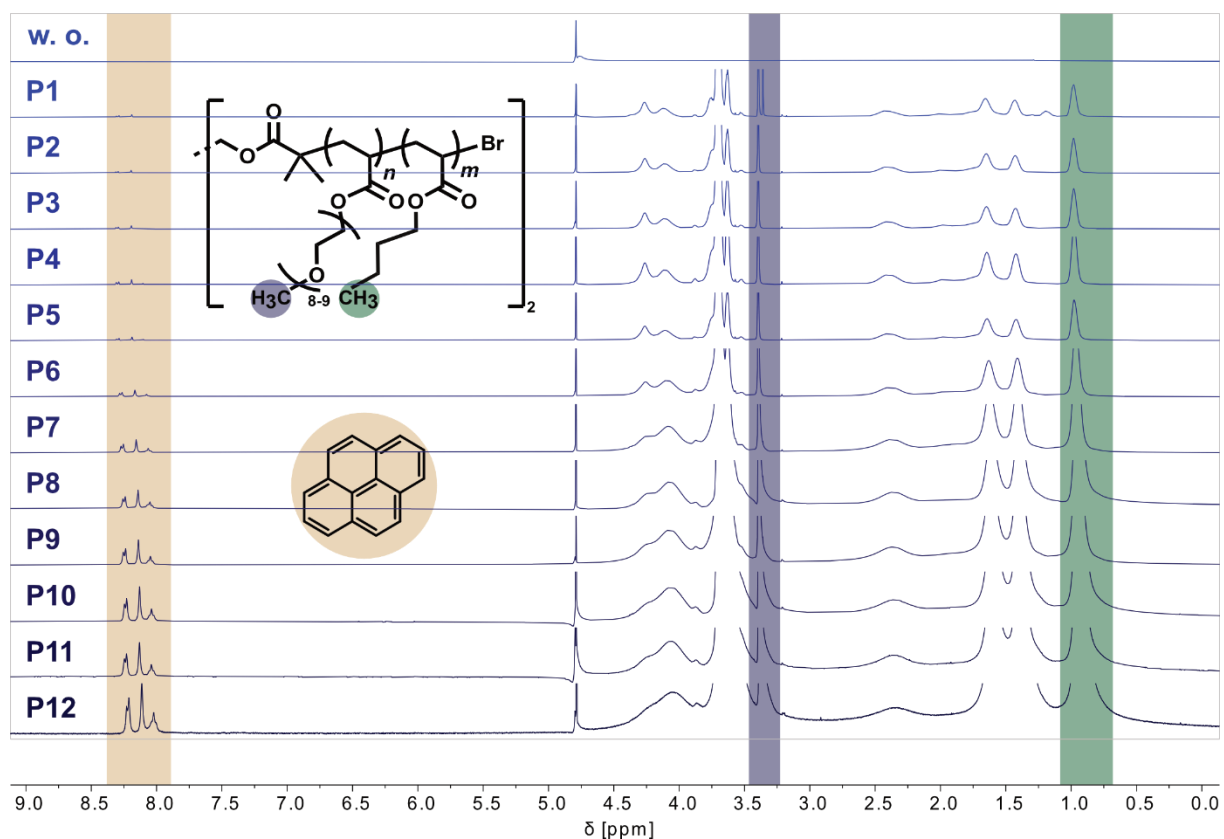


Figure S18. Representative ^1H NMR spectra of **P1-P12** saturated with pyrene in D_2O . Pyrene and polymer signals, which have been used to calculate the pyrene:polymer ratio, are indicated with colour in the spectra and the corresponding chemical structures. ($N = 2$)

Interestingly, for **P7-P12** with up to 50 encapsulated pyrene molecules per nanocarrier a significant high-field shift of the pyrene signals can be observed in the ^1H NMR spectra, attributed to the pyrene concentration increase in micellar core compared to **P1-P6**.

14. Turbidity and fluorescence measurements of pyrene-loaded micelles

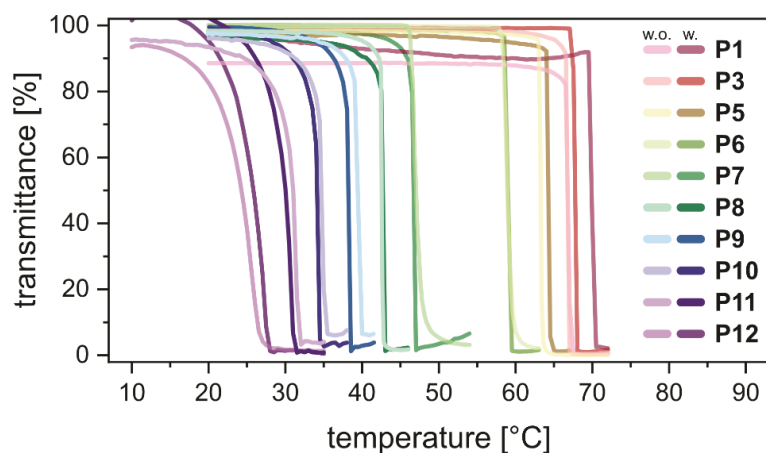


Figure S19. Representative turbidity curves of P(OEGA-co-BA) **P1-P12** in the absence (light) and presence (dark) of pyrene in PBS as a function of temperature determined at heating rates of 0.5 °C min^{-1} and a concentration of 10 mg ml^{-1} . Loading of the micelles with pyrene before the measurements was performed as described in the experimental part for capacity determination. ($n = 3$)

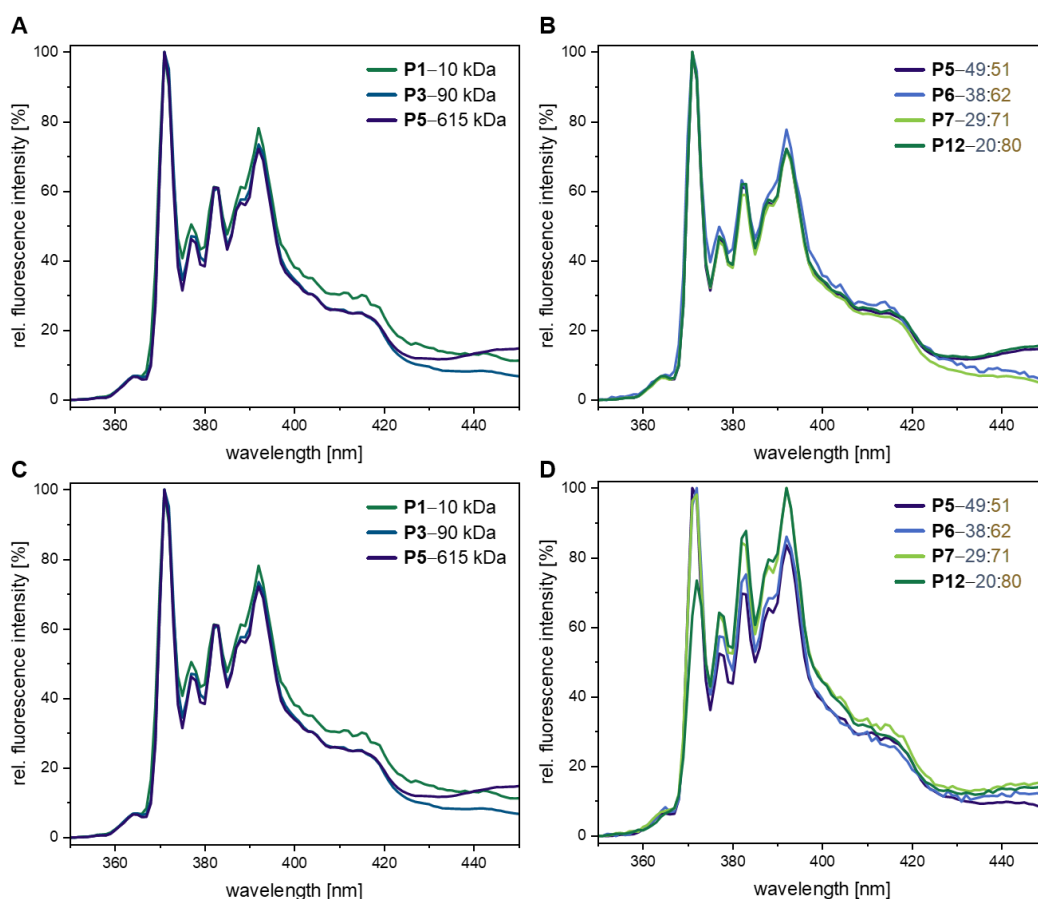


Figure S20. Fluorescence emission spectra of pyrene-loaded micelles of (A) **P1**, **P3**, and **P5** with a fixed 1:1 comonomer ratio at (A) 0.01 mg mL^{-1} , (C) 10 mg mL^{-1} and **P5-P7**, **P12** with a fixed molecular weight around 600 kDa at (B) 0.01 mg mL^{-1} , (D) 10 mg mL^{-1} in PBS at 25 °C . ($n = 3$)

Table S9. Pyrene I_1/I_3 ratio in dependence of the concentration of statistical P(OEGA-co-BA) copolymers **P1-P7** and **P12** determined via fluorescence spectroscopy at RT in PBS. ($n = 3$)

polymer	composition ^a [OEGA:BA]	I_1/I_3 ^b	I_1/I_3 ^c
P1	50:50	1.54 ± 0.05	1.62 ± 0.02
P3	50:50	1.55 ± 0.03	1.66 ± 0.02
P5	49:51	1.45 ± 0.02	1.63 ± 0.02
P6	38:62	1.31 ± 0.02	1.61 ± 0.04
P7	29:71	1.17 ± 0.01	1.69 ± 0.01
P12	20:80	0.83 ± 0.02	1.62 ± 0.01

^a molar ratio, ^b determined at a polymer concentration of 10 mg mL⁻¹, ^c determined at a polymer concentration of 0.01 mg mL⁻¹.

15. DLS measurements of pyrene-loaded micelles

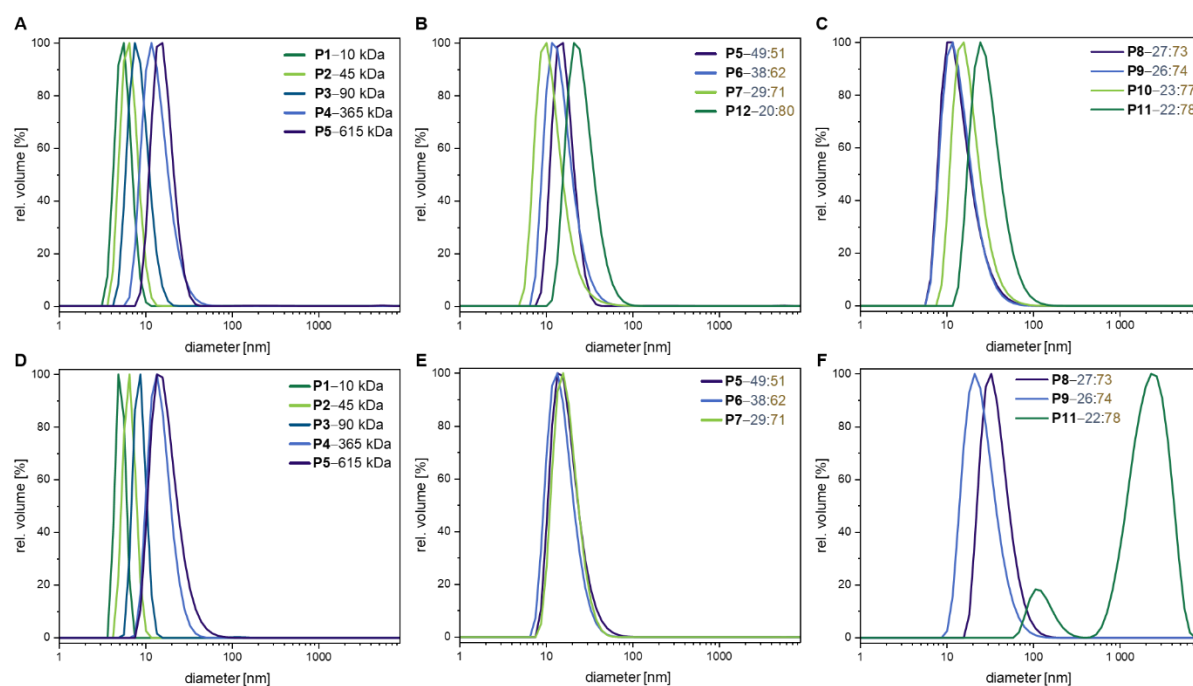


Figure S21. Representative DLS curves of P(OEGA-co-BA) copolymers **P1-P12** (10 mg mL⁻¹) saturated with pyrene grouped with respect to increasing molecular weight at a constant OEGA:BA =1:1 ratio in (A) at 25 °C and (D) at 37 °C and varying ratio of OEGA:BA at a fixed molecular weight around 600 kDa in (B,C) at 25 °C and (E,F) at 37 °C in PBS. Of note, copolymer **P10** and **P12** consistently produced unstable, large aggregates > 1 000 nm at 37 °C, which were outside the detection range of the device. ($n = 3$)

Table S10. Hydrodynamic radii R_h of statistical P(OEGA-co-BA) copolymers **P1-P12** determined from size distributions by volume curves via DLS at a concentration of 10 mg ml⁻¹ with and without pyrene loading at 25 °C in PBS. ($n = 3$)

polymer	composition ^a [OEGA:BA]	R_h^{PBS} (25 °C) [nm]	R_h^{PYR} (25 °C) [nm]
P1	50:50	2.6 ± 0.8	2.8 ± 0.6
P2	50:50	3.2 ± 1.0	3.3 ± 0.8
P3	50:50	4.3 ± 1.3	4.2 ± 1.4
P4	50:50	7.7 ± 3.0	7.0 ± 2.9
P5	49:51	8.9 ± 4.2	7.7 ± 2.9
P6	38:62	8.2 ± 3.5	7.5 ± 3.3
P7	29:71	7.4 ± 3.3	6.1 ± 3.3
P8	27:73	8.2 ± 3.6	8.1 ± 3.9
P9	26:74	9.5 ± 4.3	8.5 ± 4.2
P10	23:77	11.7 ± 6.1	9.4 ± 4.6
P11	22:78	19.2 ± 9.0	14.7 ± 7.9
P12	20:80	24.6 ± 10.0 ^b	13.3 ± 5.6 ^b

^amolar ratio. ^bdetermined by DLS at 20 °C.

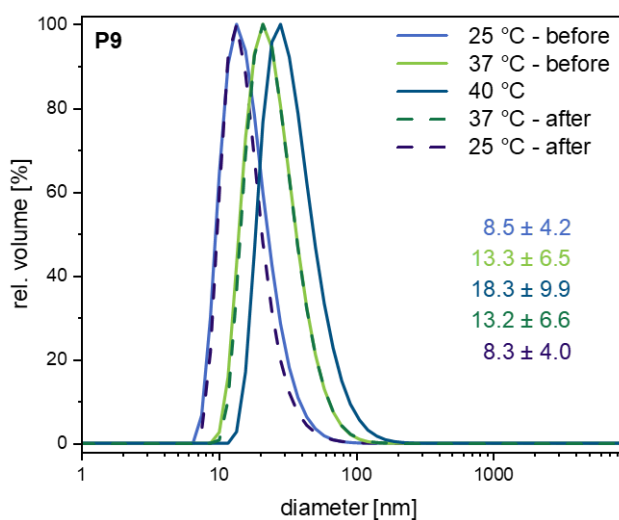


Figure S22. Representative DLS curves of **P9** (10 mg ml⁻¹) saturated with pyrene at 25 and 37 °C before exceeding the systems $T_{CP} = 38.9$ °C at 40 °C, and subsequent cooling to 37 and 25 °C. The data demonstrates the reversibility of the thermally triggered aggregation of a pyrene-loaded unimolecular micelle. ($n = 3$)

References

- [1] A. A. Kavitha, N. K. Singha, *Macromolecules*, 2010, **43**, 3193.
- [2] T. Kelen, F. Tüdös, *J. Macromol. Sci. Chem., A.*, 1975, **9**, 1.
- [3] F. Ziaee, M. Nekoomanesh, *Polymer*, 1998, **39**, 203.
- [4] M. Fineman, S. D. Ross, *J. Polym. Sci.*, 1950, **5**, 259.
- [5] F. Tüdös, T. Kelen, T. Földes-berezsnich, B. Turcsányi, *J. Macromol. Sci. A*, 1976, **10**, 1513.
- [6] H. Abdollahi, V. Najafi, F. Amiri, *Polym. Bull.*, 2021, **78**, 493.
- [7] H. Räägel, A. Turley, T. Fish, J. Franson, T. Rollins, S. Campbell, M. R. Jorgensen, *Biomed. Instrum. Technol.*, 2021, **55**, 69.
- [8] S. Imai, Y. Hirai, C. Nagao, M. Sawamoto, T. Terashima, *Macromolecules*, 2018, **51**, 398.
- [9] T. Terashima, T. Sugita, K. Fukae, M. Sawamoto, *Macromolecules*, 2014, **47**, 589.